# Lipidation effect on surface adsorption and associated fibrillation of the model protein insulin

Fogh Hedegaard, Sofie; Cardenas, Marite; Barker, Robert; Jorgensen, Lene; van der Weert, Marco

*Published in:*
Langmuir

*DOI:*
10.1021/acs.langmuir.6b00522

*Publication date:*
2016

*Document Version*
Accepted author manuscript

**Lipidation effect on surface adsorption and associated fibrillation of the model protein insulin**

Sofie Fogh Hedegaard[1], Marité Cárdenas[*2,3], Robert Barker[4], Lene Jorgensen[*1], Marco van de Weert[1]

[1]*Department of Pharmacy, Faculty of Health and Medical Sciences, University of Copenhagen, Universitetsparken 2, 2100 Copenhagen O, Denmark*

[2]*Department of Biomedical Science and Biofilms Research Center for Biointerfaces, Faculty of Health and Society, Malmo University, Per Albin Hanssons väg 35, 214 32 Malmö, Sweden.*

[3]*Department of Chemistry, Faculty of Science, University of Copenhagen, Universitetsparken 5, 2100 Copenhagen O, Denmark*

[4]*Institut Laue-Langevin, 71 avenue des Martyrs, 38042. Grenoble, Cedex 9. France. Current address: School of Science and Engineering, University of Dundee. Dundee. DD1 4HN. United Kingdom.*

* Corresponding authors:

Marité Cárdenas; Tel.: +46 40 665 74 21, e-mail: marite.cardenas@mah.se; cardenas@nano.ku.dk

Lene Jorgensen; Tel.: +45 3533 6369, e-mail: lene.jorgensen@sund.ku.dk

**ABSTRACT**

Lipidation of proteins is used in the pharmaceutical field to increase the therapeutic efficacy of proteins. In this study, we investigate the effect of a 14-carbon fatty acid modification on the adsorption behavior of human insulin to a hydrophobic solid surface and the subsequent fibrillation development under highly acidic conditions and elevated temperature by comparing to the fibrillation of human insulin. At these stressed conditions, the lipid modification accelerates the rate of fibrillation in bulk solution. With the use of several complementary surface-sensitive techniques, including quartz crystal microbalance with dissipation monitoring (QCM-D), atomic force microscopy (AFM) and neutron reflectivity (NR), we show that there are two levels of structurally different protein organization at a hydrophobic surface for both human insulin and the lipidated analogue: a dense protein layer formed within minutes on the surface and a diffuse outer layer of fibrillar structures which took hours to form. The two layers may only be weakly connected and proteins from both layers are able to desorb from the surface. The lipid modification increases the protein surface coverage and the thickness of both layer organizations.

Upon lipidation not only the fibrillation extent but also the morphology of the fibrillar structures changes from fibril clusters on the surface to a more homogenous network of fibrils covering the entire hydrophobic surface.

## INTRODUCTION

Lipidation is a common endogenous post-translational modification observed in several natural biological settings[1–3]. As a pharmaceutical tool, lipidation of peptides and proteins can be used to increase the circulation time in the bloodstream, and thus increase the therapeutic efficacy of biomolecular compounds[4–6]. However, modifying soluble proteins with a hydrophobic moiety such as a lipid tail will inevitably have an effect on the physiochemical properties of the protein, including its physical stability[7–11]. Moreover, protein drugs encounter several surfaces and interfaces during the entire lifetime of the compounds: from production, purification and storage to administration, delivery and *in vivo* utilization. Upon adsorption to solid surfaces, proteins may change conformation, potentially leading to protein unfolding [12–15]. This will in most cases result in reduced biological activity[16,17], and could moreover result in protein aggregation and fibrillation[18–21]. Indeed, surfaces are believed to be involved in the early stages of amyloid fibril development, promoting faster nucleation, probably due to increased local protein concentration near the surface[19,20,22].

Previously, the lipidated variant of the therapeutic protein glucagon-like peptide-2 (GLP-2) was shown to have high affinity for hydrophobic solid surfaces, where the attached lipid chain increased the amount of GLP-2 adsorbing per unit surface area[11]. In bulk assays, lipidation also affected the fibrillation tendency in a site-specific manner of proteins prone to form amyloid fibrils[23,24]. In the present work, we study the adsorption and subsequent fibrillation behavior of the lipidated human insulin variant $Lys^{B29}$-tetradecanoyl des-(B30) insulin, (insulin_lip), given the 14-carbon fatty acid chain covalently bound to the lysine residue (Figure 1), and we compare it to human insulin. Like several other therapeutic proteins, it is well recognized that human insulin is prone to form amyloid fibrils when applying sufficient stress to the protein in solution[25,26]. The fibrillation process can be induced and accelerated under various conditions like mechanical agitation, presence of hydrophobic surfaces, elevated temperature, and acidic pH[27,28,29]. Also the presence of a hydrophobic surface can increase the tendency of human insulin to fibrillate[18,30].

In the current study we examine for the first time the influence of a lipid chain in the

protein adsorption to hydrophobic solid surfaces and the following dynamic process of fibrillation, under acidic conditions. We compare the fibrillation kinetics for insulin_lip and human insulin in the bulk, and furthermore applied complementary surface sensitive techniques to study the surface interaction and subsequent fibrillation behavior of these proteins. We found that the lipid tail considerably increases not only the rate of fibrillation, but also the amount of initially adsorbed protein, and alters the coverage and morphology of the fibrillar species formed on the hydrophobic surface.

## MATERIALS AND METHODS

### Materials

Human insulin and $Lys^{B29}$-tetradecanoyl des-(B30) insulin, (insulin_lip) were kindly provided by Novo Nordisk A/S (Maløv, Denmark). These preparations contained 2.3 $Zn^{2+}$ ions per hexamer. Acetic acid 99-100% (glacial acetic acid), sodium chloride, ammonia solution (25%), sulfuric acid (98%), and hydrogen peroxide (30%) were obtained from Merck (Darmstadt, Germany). Hydrochloric acid (5N) and absolute ethanol (99.8%) were purchased from Prolabo (VWR International, Fontenay sous Bois, France). 3-(Trimethoxysilyl)propyl acrylate, 1-propanethiol 99%, and Thioflavin T (ThT) were obtained from Sigma-Aldrich, (Steinheim, Germany) and (3,3,3-trifluoropropyl)dimethylchlorosilane was obtained from ABCR GmbH & Co, Karlsruhe, Germany. $D_2O$ was provided by Institut Laue-Langevin (ILL), Grenoble, France. All chemicals are of analytical grade and were used without further purification. Milli-Q purified water with a resistivity of 18.2 MΩ•cm was used for all experiments.

### Preparation of insulin solutions

The protein samples were prepared immediately prior to all experiments. The proteins were dissolved in 0.1 M HCl and diluted 1:1 in volume with a freshly prepared solvent of 40 vol % acetic acid, 1 M NaCl. The solvent was filtered through a 0.2 μm sterile cellulose acetate membrane syringe filter (GVS Filter Technology, USA) to remove potential salt crystals, before mixing with the protein solutions. Protein concentration was determined using a nanodrop UV/Vis spectrophotometer (Thermo Scientific, Waltham, Massachusetts) at 276 nm applying an extinction coefficient of 6200 $M^{-1}$ $cm^{-1}$ [31].

**Thioflavin T assay**

The Thioflavin T (ThT) dye was dissolved in Milli-Q water and left to dissolve overnight at room temperature. The solution was hereafter filtered through a 0.2 µm sterile cellulose acetate membrane syringe filter (GVS Filter Technology, USA) and kept for storage at 4 °C, protected from light to avoid photobleaching. The ThT dye concentration was determined by absorbance using a molar extinction coefficient of 23,800 $M^{-1}$ $cm^{-1}$ at 412 nm[32]. The ThT fluorescence measurements were carried out using a Fluostar Optima platereader from BMG Labtechnologies (Offenburg, Germany) with 96-microwell polystyrene plates (Nunc, Roskilde, Denmark) at 35° C or 45° C, respectively. Excitation was at 450 nm and the emission intensity was recorded at 480 nm. The emission signal was measured every 400 s from the bottom of the well plate. To avoid evaporation the 96-well plate was covered with a polyolefin sealing tape. 200 µl of protein solution containing 20% acetic acid, 0.5 M NaCl, 0.05 M HCl, 20 µM ThT was added to each well and four replicates of each sample were measured.

**Surface modification**

All surfaces used in this work were modified to be hydrophobic as described below.

***Atomic force microscopy (AFM):*** New silicon (Si) wafers (100) of 0.4 x 0.4 cm size for AFM experiments were cleaned for 10 minutes in a mixture of milli-Q water, $NH_3$ (25 vol %), $H_2O_2$ (30 vol %) (5:1:1 volume ratio) heated to 75 °C. The wafers were rinsed thoroughly with both milli-Q water and ethanol, and dried in a stream of nitrogen before silanization with (3,3,3-trifluoropropyl)-dimethylchlorosilane by vapour deposition for at least 12 hours. The contact angle of modified Si wafers was measured with a Krüss G2 contact angle measuring system (Krüss GmbH, Hamburg, Germany) using the tangent method. The static contact angles of a sessile drop of milli-Q water on the crystals were >88°.

***Quartz Crystal Microbalance with Dissipation (QCM-D):*** For the QCM-D experiments standard Au sensor crystals (Biolin Scientific, Gothenburg, Sweden) were used. Prior to modification, the crystals were cleaned for 10 minutes in a mixture of milli-Q water, $NH_3$ (25 vol %), $H_2O_2$ (30 vol %) (5:1:1 volume ratio) heated to 75 °C. The Au-crystals were submersed into a 5 mM 1-propanethiol absolute ethanol solution for at least 16 hours, followed by thorough rinsing with milli-Q water and ethanol. The crystals were kept in absolute ethanol and used one day after modification. The contact angles of the modified Au-crystals were measured to >85°.

***Neutron reflectivity:*** To remove any trace of organic contaminants, the polished Si crystals (111) were cleaned for 10 minutes in a 80 °C diluted piranha solution of milli-Q water, $H_2SO_4$ (98 vol

%) and $H_2O_2$ (25 vol %) in a 5:4:1 volume ratio, before modification with 3-(trimethoxysilyl)propyl acrylate by vapour deposition for at least 6 hours, giving a contact angle >70° . Hereafter, the crystals were sonicated in milli-Q water and absolute ethanol and dried in a stream of nitrogen before use.

Although the surface chemistry is different for the three methods, the surface wettability is similar, and thus the surfaces are expected to behave similar in terms of protein adsorption[33].

**Atomic force microscopy**

AFM imaging was performed with a Nanoscope IV multimode AFM (Veeco Instruments Inc., Santa Barbara, CA) in Peak Force Quantitative Nanomechanical Mapping (QNM) tapping mode in air. A silicon tip mounted on a silicon nitride cantilever (SCANASYST-AIR, Bruker, USA) with a spring constant of 0.4 N/m and a resonance frequency of 70 kHz was used for high-resolution images of soft samples. Modified Si wafers were incubated without agitation in a 300 µl protein solution of 20 vol % acetic acid, 0.5 M NaCl, 0.05 M HCl at 35 °C or 45 °C, for insulin_lip and human insulin, respectively. At each time point a Si wafer was removed from the protein solution, rinsed with milli-Q water, and dried in a stream of nitrogen. All images were recorded with 512 x 512 pixel resolution and captured with a scan rate of 1 Hz. The z-setpoint and feedback gains were optimized manually during each scan. The images were analysed and processed in the Gwyddion 2.36 software.

**Quartz Crystal Microbalance with Dissipation monitoring**

The QCM-D experiments were carried out with a Q-SENSE E4 system (Q-Sense, Västra Frölunda, Sweden). The fundamental frequency (5 MHz) and six overtones ($3^{rd}$, $5^{th}$. $7^{th}$, $9^{th}$, $11^{th}$, and $13^{th}$) were found and recorded in milli-Q water. The flow cells were connected to a peristaltic pump (Ismatec IPC, Glattbrugg, Switzerland) employing a flow rate of 100 µL/min. Before measurements, the temperature was equilibrated to 35 °C or 45 °C, respectively. The protein solutions were continuously flowed through the cells for 15 minutes; hereafter the system was left for incubation of the proteins under no flow conditions. For calculation of Sauerbrey thickness a protein density (ρ) of 1.33 g/cm$^2$ was applied[34].

**Neutron reflectivity**

Specular neutron reflectivity measurements were performed at the Institut Laue-Langevin (ILL, Grenoble, France) at the two reflectometers D17[35] and Figaro[36], recording time-of-flight

reflectivity. The specular reflection R(Q) is measured as a function of the wave-vector transfer perpendicular to the surface, $Q=(4\pi/\lambda)\sin\theta$, where $\lambda$ is the wavelength of the incident beam and $\theta$ is the angle between the incoming beam and the reflecting surface. The temperature was controlled using a water bath at either 35 or 45 °C. All NR profiles were analyzed using Motofit reflectivity analysis software[37].The scattering length density (SLD), the thickness (*d*), solvent penetration ($\varphi$) and interfacial roughness between the layers ($\sigma$) were the parameters used to characterize the $SiO_2$, the hydropbobic silane layer and the protein layer.

## RESULTS & DISCUSSION

### Lipidation accelerates the fibrillation process in bulk solution

Fibril formation of insulin_lip and human insulin in bulk solution was monitored by ThT fluorescence, a commonly used assay to detect amyloid fibrils in which the dye ThT forms a highly fluorescent complex with amyloid fibrils, which enables the detection of the existence and rate of formation of fibrils[28,32]. The fibrillation was studied in a highly acidic solution (pH 1.8) containing a large amount of acetic acid, in which human insulin is in the monomeric form[38]. This significantly increases the fibrillation rate as compared to a human insulin solution at neutral pH. Insulin_lip has a lower self-association property than the native insulin at neutral pH, possibly due to binding of the lipid chain to the dimer interface[8], and thus likely also is a monomer under the acidic conditions employed here. However, we cannot rule out that multimerization through the lipid chains takes place.

In Figure 2 the ThT fluorescence is presented as a function of incubation time for the proteins insulin_lip and human insulin at 35 °C and 45 °C, respectively. The kinetic curves displayed the characteristic sigmoidal profile, with a lag phase followed by a sudden increase in the ThT fluorescent signal. As expected[39], increasing the temperature from 35 °C and 45 C accelerated the fibril development for both protein variants, while the lipid tail dramatically increased the rate of fibril formation, regardless of temperature.

Fibrillation is known to be a stochastic process, and thus variability in the onset of fibrillation is not uncommon[28]. In this study, the onset of fibrillation for human insulin is also observed to vary notably between replicates. However, for insulin_lip the fibrillation reproducibility was higher than for human insulin, suggesting an effect of the lipid tail on the initial stages of fibrillation for this protein. Given the noteworthy difference in lag times of

fibrillation between the two proteins at equal temperature, and with the assumption that the temperature affects only the kinetics of the fibrillation process, the experiments described hereafter are performed at 35 °C for insulin_lip and at 45 °C for human insulin, respectively. In this way comparable fibrillation kinetics for the two protein variants was achieved within a convenient time frame (ca. 8 hours).

**AFM shows difference in fibril morphology and surface coverage on hydrophobic surfaces**

AFM is a widely used tool to visualize biological systems on the nanoscale, and has previously been used to image fibrillar structures on various surfaces[20,40]. Although AFM does not provide absolute heights or layer thickness, it gives information about relative differences in heights or layer thicknesses and this is useful for comparative studies as performed here. Figure 3 and 4 show the time-lapse tapping AFM images recorded in air of insulin_lip and human insulin, respectively. The timing for fibril development observed on the surfaces was similar to the fibrillation kinetics observed for bulk samples monitored by ThT binding, with insulin_lip fibrillating faster than human insulin, (Figure 2). As shown in Figure 3, adsorbed insulin_lip molecules covered the entire surface within 10 minutes of protein exposure, and the initial development of fibrillar structures was observed after 3 hours of incubation. The mature fibrils of insulin_lip formed a large network that covered the entire surface, growing in thickness over time and approaching an apparent maximum thickness of 1 μm at the core clusters of the fibrils. In contrast, human insulin adsorbed with a notably lower total surface coverage than insulin_lip and the mature fibrils occurred as clusters covering only minor parts of the surface area (Figure 4).

It is clear that the lipid tail affects not only the extent of adsorption, but also the morphology and coverage of the fibrillar species. However, the structural arrangements of the proteins on the surface visualized with AFM could possibly have been affected by the rinsing and subsequent drying step of the proteins-incubated hydrophobic surfaces, prior to imaging. For example, the rinsing step could have removed loosely bound protein from the surface, affecting the observed human insulin surface coverage. Despite such artifacts, the AFM data supports the hypothesis that the hydrophobic lipid moiety has a strong affinity for the hydrophobic surface, and this strong interaction may influence the further development of surface associated protein fibrils. For both protein variants, AFM also suggests two levels of organization: an inner, thin and dense layer as well as an outer, thick and more diffuse layer of fibrils. The diffuse outer layer grows slowly with time while the inner dense layer form within minutes. It is not possible to

determine from these images whether the organization of these two layers is strongly interconnected.

**QCM-D data shows that both the initial layer and fibril layer are structurally different**

QCM-D allows the study in real time of both the extent of the initial protein adsorption at the solid-liquid interface *in situ*, and the structural rearrangements that follow, leading to the formation of fibrils on the sensor surface. The Sauerbrey equation[41] is commonly applied for rigid adsorbed layers, and a modified version of the equation can be used for calculation of the layer thickness:

$$d_{eff} = -\frac{C}{n \cdot \rho} \cdot \Delta f$$

$d_{\mathrm{eff}}$ denoting the effective layer thickness, ρ the density of the layer, $n$ is the overtone number, $f$ the frequency and the mass sensitivity constant $C$ = 17.7 ng cm$^2$ Hz$^{-1}$ at the fundamental frequency; $f$=5 MHz. For a typical adsorption process, the frequency decreases, whereas an increase in frequency will be expected for a desorption process. Reconfiguration of the deposited protein layer is accompanied with a change in the viscoelastic properties, which is monitored in the dissipation value. The QCM-D results for insulin_lip and human insulin are depicted in Figure 5, where shifts in frequency ΔF and dissipation ΔD of three overtones (5$^{\mathrm{th}}$, 7$^{\mathrm{th}}$, and 9$^{\mathrm{th}}$) are plotted as a function of elapsed time.

Upon exposure of insulin_lip to the hydrophobic modified surface, an initial decrease to -26 Hz occurred. However, no lasting initial adsorption stage plateau occurred (Figure 5A, dashed box). The calculated Sauerbrey thickness for the initial adsorbed protein layer (35 Å) suggests immediate double layer formation or adsorption of the protein in a dimeric, extended or higher organized state. Both QCM-D signals changed significantly during the hours of the experiment while the overtones spread significantly within the first hour of incubation, indicating that the initially adsorbed protein layer rearranges continuously during the entire duration of the experiment, forming a less dense layer with notable increased viscoelastic properties.

For human insulin, on the other hand, the initial adsorption phase (Figure 5B, dashed box) reached a steady state at approximately -12 Hz that corresponds to a Sauerbrey thickness of 16 Å. This indicates that after the initial protein monolayer formation no further apparent change at the interface occurred within the first three hours of incubation time. After these three hours, a dramatic change in both QCM-D signals was observed including large spreading of the overtones. Thus, the adsorbed layer cannot be described as rigid from this point onwards. Noteworthy is that at this point the frequency shifted from negative to positive values before

reaching a steady state. This situation is counterintuitive considering normal mass loading theory, where positive frequency values indicate mass loss. The same trend of frequency changes has been reported by Hovgaard et al.[42] for glucagon fibrillation. Similar to our results, they observed a characteristic lag period with negative frequency values, followed by a sudden increase to positive values upon fibril growth. The adhesion of bacteria[43] and colloids[44,45] to surfaces has also been reported to cause positive frequency shifts. In the latter cases, a coupled resonance model has been used to explain the positive frequency values observed. The model was first suggested by Dybwad for spheres in the dry state[46], but was shown also to be plausible for colloids in liquid phase media[47]. According to this model, large colloidal objects in the micrometer size range, that adsorb weakly via few contact points to the sensor surface, could form a second resonator with its own frequency. Positive frequency shifts can then be observed when the effective rigidity of this coupled resonator increases. The coupled resonance model is not limited to spherical particles[47], and thus coupled resonance could occur also with larger objects with different geometries, such as fibrillar structures, weakly coupled to the sensor surface. As observed on the AFM images, human insulin tends to form clusters of fibrillar structures on the surface. Possibly these clusters are only weakly connected to the surface and thus act as a second resonator explaining the positive frequency values observed for human insulin.

Shifts in the QCM-D signal of higher overtones are associated with changes occurring near the sensor surface, whereas shifts in the lower overtones correspond to processes occurring closer to the solvent interface, i.e. far away from the sensor surface. The largest signal shifts in the data (Figure 5) occurred for the lowest overtone plotted ($5^{th}$), indicating that the most drastic events (the reconfiguration into fibrillar structures) take place in the solvent-protein interface. Thus, the fibrils are probably grown in solution rather from within the initial layer of adsorption regardless of the protein variant, although protein molecules desorbing from the surface could participate in the fibrillation process. In summary, on the basis of the coupled resonance model, we suggest that human insulin fibrils are weakly associated to the hydrophobic surface while insulin_lip likely exhibits stronger adhesion to the surface.

**Neutron reflectivity data suggests that the inner protein layer and the fibrillar structures are weakly connected**

Neutron reflectivity (NR) allows the study of buried protein structures perpendicular to the surface plane. In this work, NR measurements were performed in order to examine in detail the structure of the protein layers. After a full characterization of the clean silane-modified substrate in $H_2O$ and $D_2O$, protein adsorption to the surface was measured in $H_2O$. Despite poorer isotropic

contrast, we performed the NR experiments in $H_2O$ in order to avoid unknown deuteration effects in the fibrillation process. Figure 6 presents the NR profiles of insulin_lip and human insulin measured as a function of Q. Upon initial adsorption of insulin_lip to the surface, the NR profile changed reflecting the adsorption event. Applying a three-layer model ($SiO_2$/silane/protein), the initially formed protein layer thickness of insulin_lip was fitted to a value of 53 Å, with a surface coverage of 28 % (v/v). Although the NR thickness is larger than the QCM-D Sauerbrey thickness, the data confirms that insulin_lip adsorbs in a double or multilayer layer arrangement, potentially in an extended structural conformation. After incubation of the protein for 6 h, the minimum in the NR curve shifted to lower Q, implying a thickening of the protein layer. Indeed, the layer was fitted to a value of 69 Å having a surface coverage of 23% (v/v). Such thickness increase of the inner protein layer over time was not a consequence of increase in the protein surface coverage during incubation, but rather due to a real thickening of the protein layer since a good fit couldn't be obtained by varying the coverage parameter alone while keeping the protein layer thickness fixed. Indeed, the surface coverage decreases slightly over time (28 to 23%). However, both the initial and final inner protein adsorbed layers have similar protein densities (proportional to the surface coverage times the layer thickness). This would suggest a redistribution or reorganization of the inner protein layer, with little water being expelled from this layer. The NR profiles did not show any obvious sign of the presence of a second layer of fibrillar structures after long incubation time (kiessig fringes), but instead a shift in the intensity of the NR profiles occurred over time. This shift can be attributed to a change in the SLD of a near surface adsorbed diffuse layer of fibrils in solvent, which are thick enough to be considered as the bulk layer by the incoming neutrons. A more detailed discussion of this phenomenon for specular neutron reflection from relatively thick interfaces can be found elsewhere[48]. It is also possible to model this shift as a fourth protein layer that is at least 500 Å thick and 200 Å rough (above these values there was no sensitivity in the reflectivity to these parameters), which support the hypothesis of a very thick-diffuse surface adsorbed layer of fibrils. Our best fit suggests that 20 % (v/v) of this near surface bulk layer was covered by fibrils, while the coverage of the initial formed inner protein layer decreases slightly during 6 hours of incubation, but increased in layer thickness. The latter suggests protein redistribution within the adsorbed layer with minor net desorption from the surface. Upon rinsing with solvent after protein incubation, most of the inner protein layer was removed from the surface, whereas the diffuse near surface layer only decreased by 50 % to a final fibrillar content of 10 % (v/v). This suggests that the fibril layer was partially reversibly bound while the inner layer was fully reversibly bound to the surface. Therefore, the two protein layers act as independent layers.

The NR profiles on human insulin suggest minor adsorption of protein, even after eight hours of incubation at 45 °C (Figure 6B), and rinsing with $H_2O$ resulted in complete removal of protein from the surface (not shown). For human insulin it was not possible to fit both protein layer thickness and coverage at the same time, using only the $H_2O$ contrast. Therefore the protein layer thickness was fixed to 16 Å based on our QCM-D results using the Sauerbrey equation, a value which is in the same order of previous obtained SAXS data on human insulin under similar conditions[38]. The coverage was allowed to vary, resulting in a value of ~17% (v/v) after eight hours of incubation. In the fitting procedure, the roughness parameter was fixed to 1Å for all layers since the quality of the fit was insensitive to changes in roughness below 5Å. Besides the expected SLD change for the acetic acid – $H_2O$ mixture as compared to pure $H_2O$, there was no obvious effect on the SLD value of the bulk solution upon human insulin fibrillation, in contrast to insulin_lip.

The AFM data suggest that the surface coverage of human insulin fibrils was low, with the fibrils arranged in clusters. This observation explains both the QCM-D data according to the coupled resonance model, and the lack of changes in the NR profile upon long incubation time. We can, however, confirm the presence of fibrils in the NR experiments for both protein variants as they were visually observed as a turbid sample solution upon dismounting the flow cell at the end of the experiment. Furthermore, AFM images showed that the insulin_lip fibrils covered the entire surface, forming a homogenous fibrillar network. This explains the typical QCM-D traces for adsorption processes observed in this case, and furthermore also explains the significant change in the SLD value of the bulk solvent upon protein incubation observed in the NR experiment. Together, our data suggests that fibrils are formed in solution rather than emerging from the surface. However, we cannot rule out that possible changes in protein conformation upon adsorption and desorption may contribute to fibril growth.

## CONCLUSION

Under acidic conditions, where the proteins are likely to exist as monomers, a lipid tail attached to human insulin accelerates the fibrillation process in bulk regardless of temperature (35 and 45 °C). On hydrophobic modified surfaces, two levels of structural organization of the protein layers were observed. Results from AFM, QCM-D, and NR suggest that a dense, thin layer formed within minutes, the thickness of which depended on the presence of the lipid tail. For insulin_lip,

this protein layer changed and turned thicker over time. Additionally, a second thick and less dense layer that corresponds to fibrillar structures formed over hours. Both the morphology and coverage of the fibrils depended on the lipid tail, with the non-lipidated human insulin forming isolated fibril clusters on the surface, while insulin_lip covered the entire surface with an extended fibril network. For both proteins, it appears that the two levels of organization in the protein layers are only weakly connected, suggesting that the second layer of fibrillar structures grows from insulin monomers in solution, rather than directly forms within the initial formed dense protein layer. The fact that the protein layers can be desorbed and that the protein layer coverage decreased over time (at least for insulin_lip) suggests that these layers are quite dynamic, and desorbed protein could contribute to fibril formation. In conclusion, the lipid tail affects not only the rate of fibrillation but also the initial adsorbed state and the coverage and structure of the fibrils on a hydrophobic surface.

**ACKNOWLEDGEMENTS**

The authors would like to thank Novo Nordisk A/S for providing the human insulin and the lipidated insulin analogue used in this study.

This project was partly funded by the UCPH2016 project CoNeXT.

The Drug Research Academy, University of Copenhagen, provided funding for the nanodrop UV/Vis spectrophotometer, while the Fluostar Optima platereader was funded by the Alfred Benzon Foundation and the Drug Research Academy, University of Copenhagen.

We thank ILL for the allocation of beam time (experiment 8-02-701 & TEST-2429), the associated data can be downloaded at the links provided below:

Cardenas, Marite; Barker, Robert; Hedegaard, Sofie; Jagalski, Vivien and Sotres, Javier. (2014). Terpenoids: their effect on biological membranes. Institut Laue-Langevin (ILL) doi:10.5291/ILL-DATA.8-02-701

Cardenas, Marite; Barker, Robert and Hedegaard, Sofie. (2014). Insulin adsorption to hydrophobised surfaces. Institut Laue-Langevin (ILL) doi:10.5291/ILL-DATA.TEST-2429

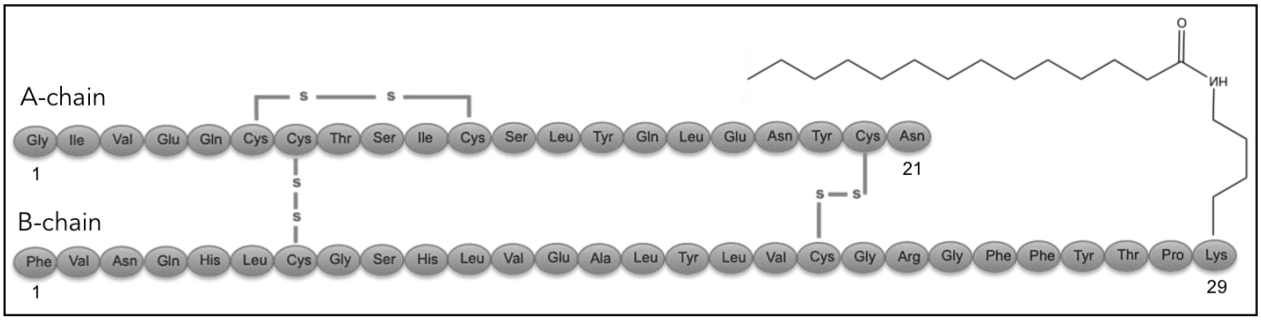


**Figure 1:** Primary structure of lipidated human insulin analogue $Lys^{B29}$-tetradecanoyl des-(B30) insulin, (insulin_lip).

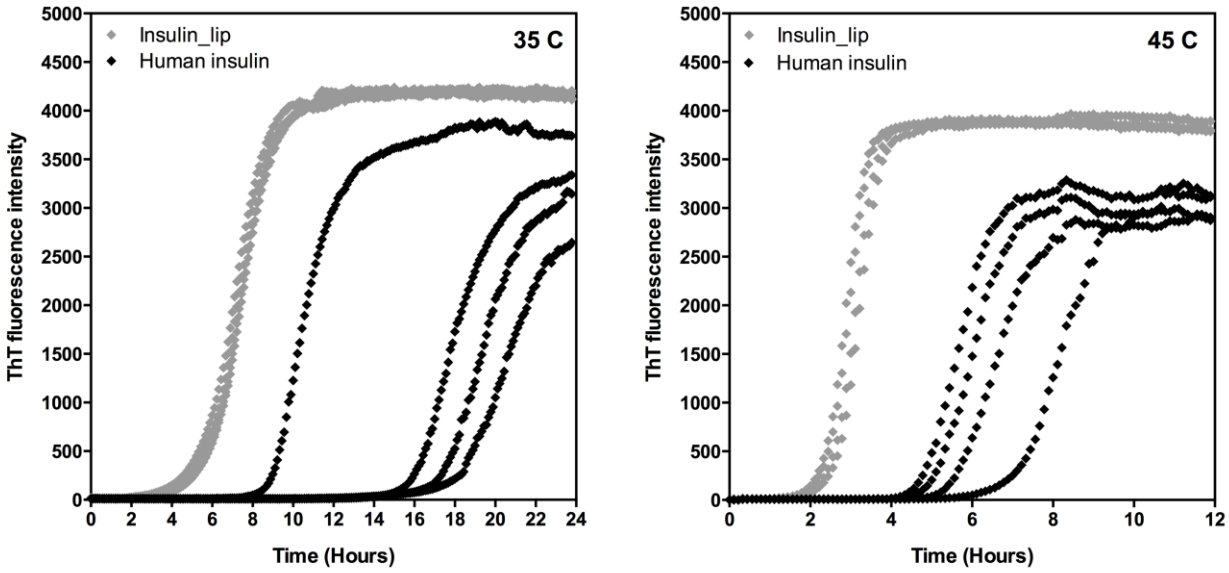


**Figure 2:** Kinetics of four replicates of human insulin and insulin_lip fibrillation in 20% acetic acid, 0.5 M NaCl, 0.05 M HCl at 35 °C (left) and 45 °C (right), respectively ($\lambda_{ex}$ = 450 nm, $\lambda_{em}$ =480 nm). Protein concentration is 2.5 mg/ml.

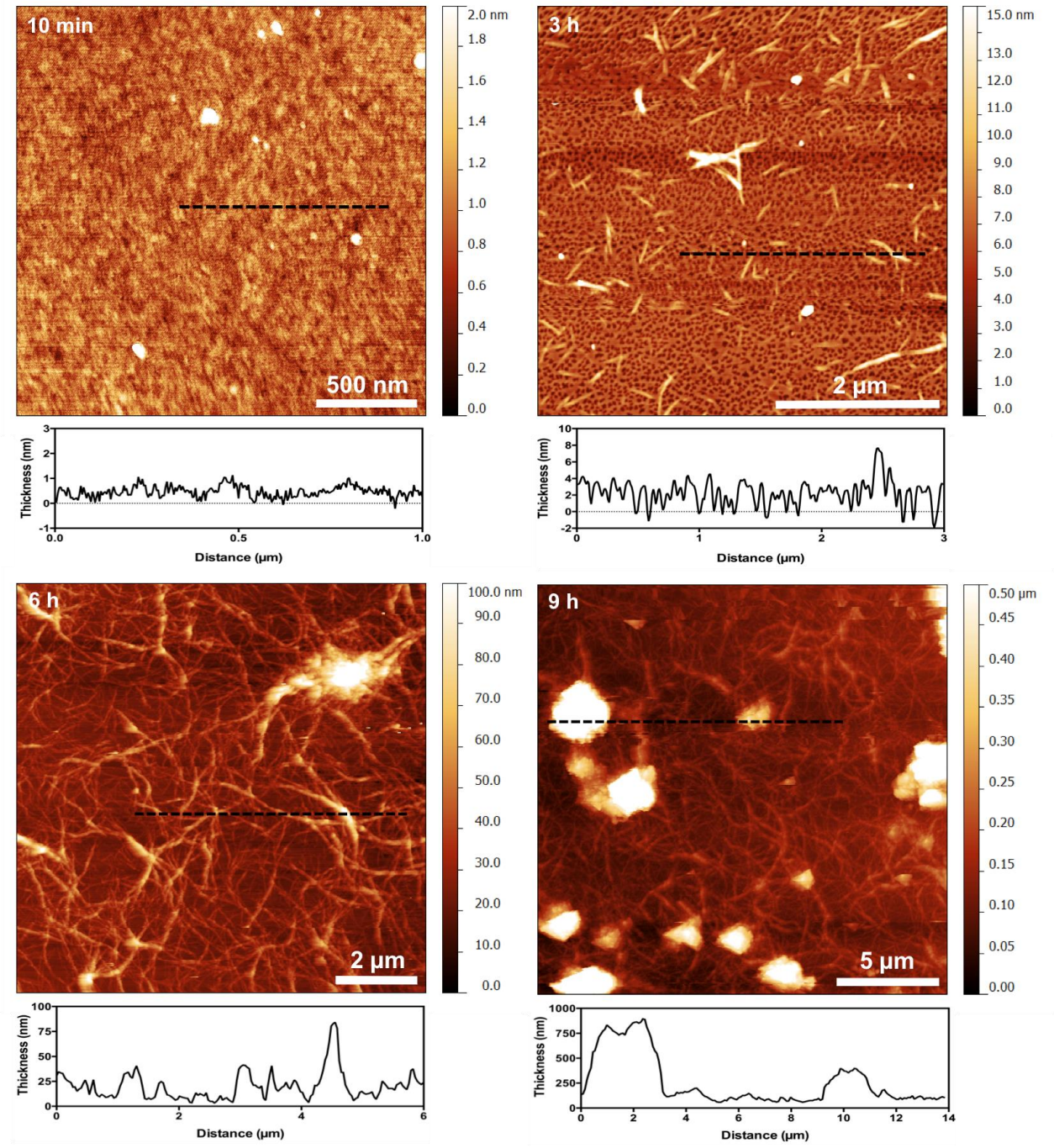


**Figure 3:** Tapping mode AFM height images (in air) of hydrophobic modified Si wafers exposed to insulin_lip solutions of 2.5 mg/ml at 35 °C, upon various incubation times. The surfaces were rinsed with milli-Q water and dried with $N_2$ before imaging. The black dashed lines in the images correspond to the height profiles below the AFM image. For a clean modified Si wafer imaged in air, see Supplementary information (Figure S1).

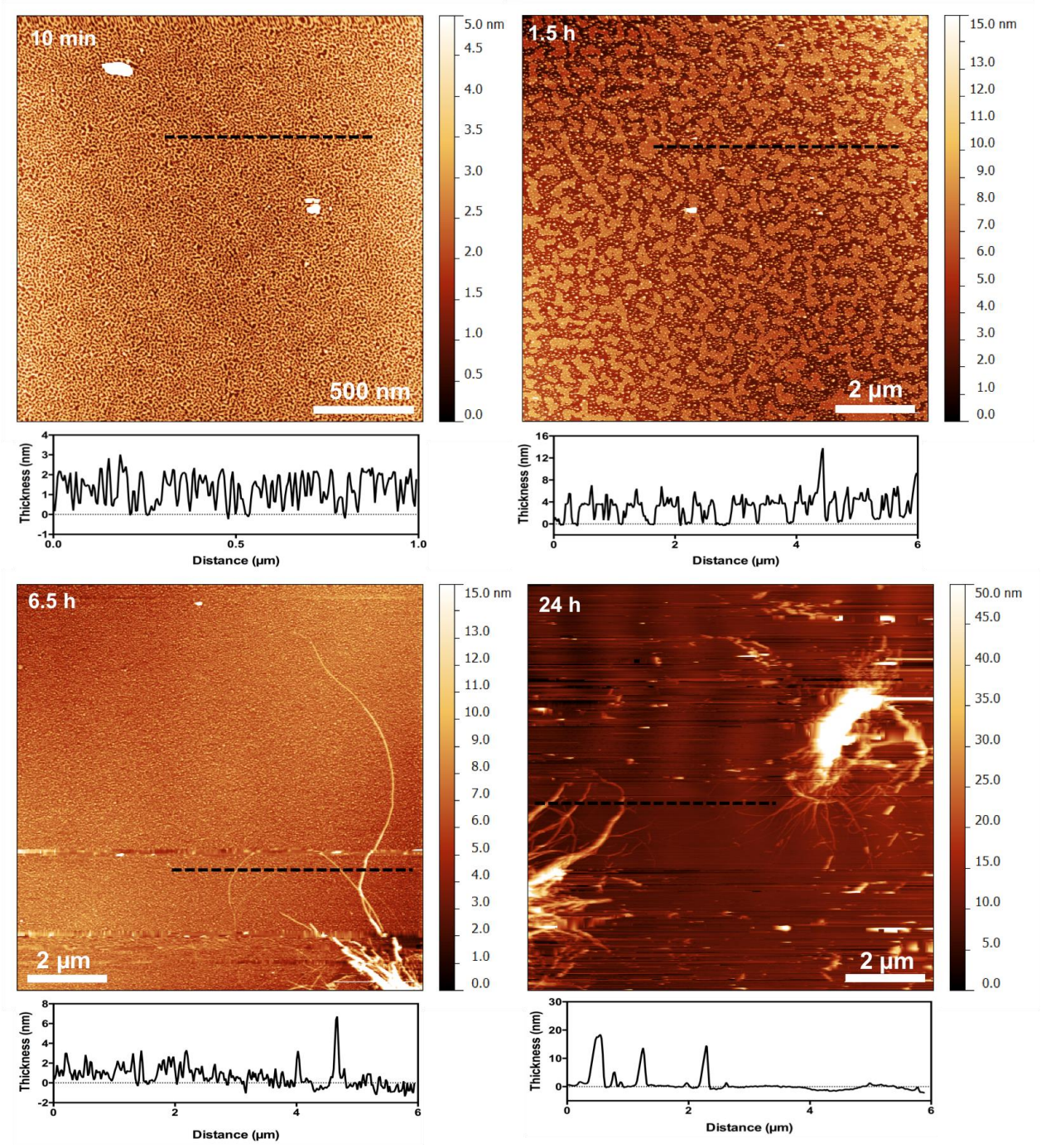


**Figure 4:** Tapping mode AFM height images (in air) of hydrophobic modified Si wafers exposed to human insulin solutions of 2.5 mg/ml at 45 °C, upon various incubation times. The surfaces were rinsed with milli-Q water and dried with $N_2$ before imaging. The black dashed lines in the images correspond to the height profiles below the AFM image. For a clean modified Si wafer imaged in air, see Supplementary information (Figure S1).

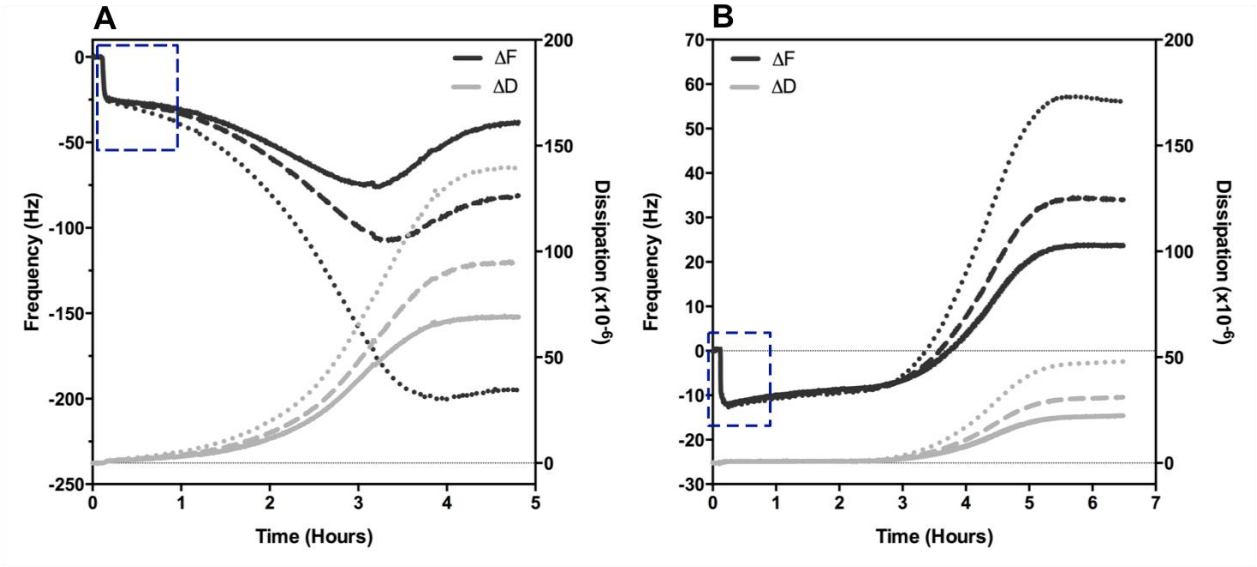


**Figure 5:** Representative QCM-D traces from a typical experiment of A: insulin_lip at 35 °C and B: human insulin at 45 °C, respectively. The frequency (ΔF) and dissipation (ΔD) shifts divided by overtones: 5 (dotted line), 7 (dashed line), and 9 (solid line) are displayed as a function of protein exposure time. The protein solutions are continuously flowed through the cells at 100 µl/min for 15 min and then the system is left to equilibrate under no flow conditions. n=3. The dashed boxes indicate the level of initial adsorption. Protein concentration is 2.5 mg/ml.

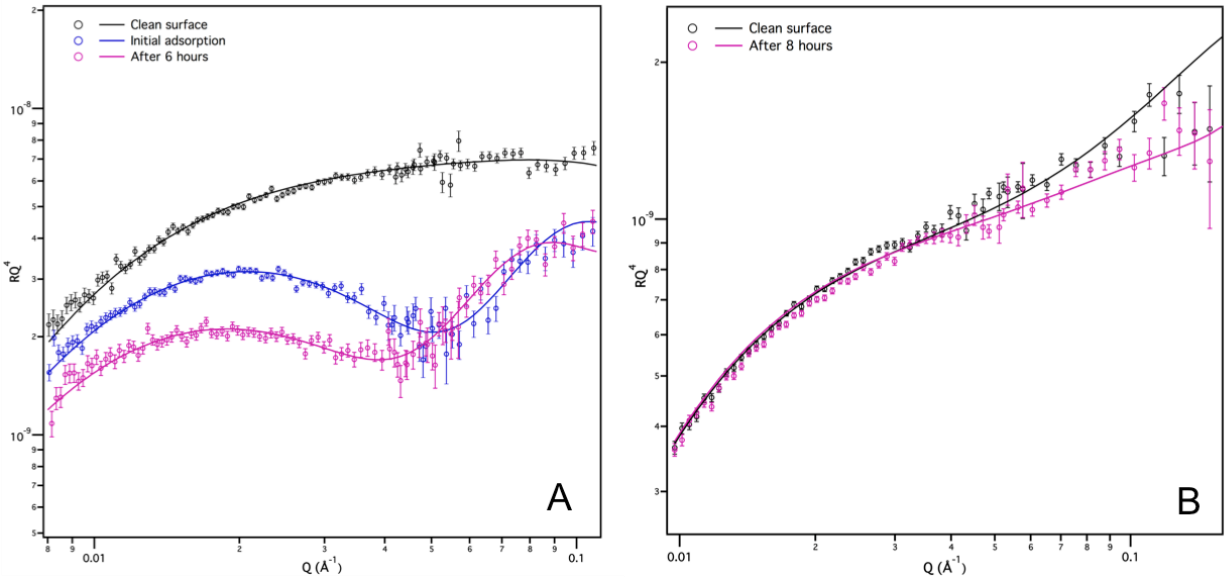


**Figure 6:** Neutron reflectivity profiles of a silane-modified surface in $H_2O$ contrast, before and after adsorption of 2.5 mg/ml insulin_lip (A) and human insulin (B). The lines are best corresponding fits to the data. The error in the SLD of the bulk after protein incubation is 14%, while the errors in the thin protein layer thickness, coverage and roughness are lower than 5%, 10% and 20% respectively.

## REFERENCES


(1) Kang, R.; Wan, J.; Arstikaitis, P.; Takahashi, H.; Huang, K.; Bailey, A. O.; Thompson, J. X.; Roth, A. F.; Drisdel, R. C.; Mastro, R.; *et al.* Neural Palmitoyl-Proteomics Reveals Dynamic Synaptic Palmitoylation. *Nature* **2008**, *456*, 904–909.

(2) Aicart-Ramos, C.; Valero, R. A.; Rodriguez-Crespo, I. Protein Palmitoylation and Subcellular Trafficking. *Biochim. Biophys. Acta - Biomembr.*, **2011,** *1808*, 2981–2994.

(3) Martin, B. R.; Cravatt, B. F. Large-Scale Profiling of Protein Palmitoylation in Mammalian Cells. *Nat. Methods* **2009**, *6*, 135–138.

(4) Knudsen, L. B.; Nielsen, P. F.; Huusfeldt, P. O.; Johansen, N. L.; Madsen, K.; Pedersen, F. Z.; Thøgersen, H.; Wilken, M.; Agersø, H. Potent Derivatives of Glucagon-like Peptide-1 with Pharmacokinetic Properties Suitable for Once Daily Administration. *J. Med. Chem.* **2000**, *43*, 1664–1669.

(5) Havelund, S.; Plum, A.; Ribel, U.; Jonassen, I.; Vølund, A.; Markussen, J.; Kurtzhals, P. The Mechanism of Protraction of Insulin Detemir, a Long-Acting, Acylated Analog of Human Insulin. *Pharm. Res.* **2004**, *21*, 1498–1504.

(6) Martin, C. M. A.; Irwin, N.; Flatt, P. R.; Gault, V. A. A Novel Acylated Form of (D-Ala2)GIP with Improved Antidiabetic Potential, Lacking Effect on Body Fat Stores. *Biochim. Biophys. Acta - Gen. Subj.* **2013**, *1830*, 3407–3413.

(7) Longo, E.; Santis, E. De; Hussain, R.; Walle, C. F. Van Der; Casas-Finet, J.; Uddin, S.; Dos, A. The Effect of Palmitoylation on the Conformation and Physical Stability of a Model Peptide Hormone. *Int. J. Pharm.* **2014**, *472*, 156–164.

(8) Olsen, H. B.; Kaarsholm, N. C. Structural Effects of Protein Lipidation as Revealed by LysB29-Myristoyl, des(B30) Insulin. *Biochemistry* **2000**, *39*, 11893–11900.

(9) Ward, B. P.; Ottaway, N. L.; Perez-Tilve, D.; Ma, D.; Gelfanov, V. M.; Tschöp, M. H.; DiMarchi, R. D. Peptide Lipidation Stabilizes Structure to Enhance Biological Function. *Mol. Metab.* **2013**, *2*, 468–479.

(10) Pinholt, C.; Hostrup, S.; Bukrinsky, J. T.; Frokjaer, S.; Jorgensen, L. Influence of Acylation on the Adsorption of Insulin to Hydrophobic Surfaces. *Pharm. Res.* **2011**, *28*, 1031–1040.

(11) Pinholt, C.; Kapp, S. J.; Bukrinsky, J. T.; Hostrup, S.; Frokjaer, S.; Norde, W.; Jorgensen, L. Influence of Acylation on the Adsorption of GLP-2 to Hydrophobic Surfaces. *Int. J. Pharm.* **2013**, *440*, 63–71.

(12) Haynes, C. A.; Norde, W. Structures and Stabilities of Adsorbed Proteins. *J. Colloid Interface Sci.* **1995**, *169*, 313–328.

(13) Mollmann, S. H.; Jorgensen, L.; Bukrinsky, J. T.; Elofsson, U.; Norde, W.; Frokjaer, S. Interfacial Adsorption of Insulin Conformational Changes and Reversibility of Adsorption. *Eur. J. Pharm. Sci.* **2006**, *27*, 194–204.

(14) Li, S.; Leblanc, R. M. Aggregation of Insulin at the Interface. *J. Phys. Chem. B* **2014**, *118*, 1181–1188.

(15) Roach, P.; Farrar, D.; Perry, C. C. Interpretation of Protein Adsorption: Surface-Induced Conformational Changes. *J. Am. Chem. Soc.* **2005**, *127*, 8168–8173.

(16) Zoungrana, T.; Findenegg, G.; Norde, W. Structure, Stability, and Activity of Adsorbed Enzymes. *J. Colloid Interface Sci.* **1997**, *190*, 437–448.

(17) Norde, W.; Zoungrana, T. Surface-Induced Changes in the Structure and Activity of Enzymes Physically Immobilized at Solid/liquid Interfaces. *Biotechnol. Appl. Biochem.* **1998**, *28*, 133–143.

(18) Nault, L.; Guo, P.; Jain, B.; Bréchet, Y.; Bruckert, F.; Weidenhaupt, M. Human Insulin Adsorption Kinetics, Conformational Changes and Amyloidal Aggregate Formation on Hydrophobic Surfaces. *Acta Biomater.* **2013**, *9*, 5070–5079.

(19) Zhu, M.; Souillac, P. O.; Ionescu-Zanetti, C.; Carter, S. A.; Fink, A. L. Surface-Catalyzed Amyloid Fibril Formation. *J. Biol. Chem.* **2002**, *277*, 50914–50922.

(20) Nayak, A.; Dutta, A. K.; Belfort, G. Surface-Enhanced Nucleation of Insulin Amyloid Fibrillation. *Biochem. Biophys. Res. Commun.* **2008**, *369*, 303–307.

(21) Perevozchikova, T.; Nanda, H.; Nesta, D. P.; Roberts, C. J. Protein Adsorption, Desorption, and Aggregation Mediated by Solid-Liquid Interfaces. *J. Pharm. Sci.* **2015**, *104*, 1946–1959.

(22) Smith, M. I.; Sharp, J. S.; Roberts, C. J. Nucleation and Growth of Insulin Fibrils in Bulk Solution and at Hydrophobic Polystyrene Surfaces. *Biophys. J.* **2007**, *93*, 2143–2151.

(23) Qahwash, I. M.; Boire, A.; Lanning, J.; Krausz, T.; Pytel, P.; Meredith, S. C. Site-Specific Effects of Peptide Lipidation on Beta-Amyloid Aggregation and Cytotoxicity. *J. Biol. Chem.* **2007**, *282*, 36987–36997.

(24) Rawat, A.; Nagaraj, R. Covalently Attached Fatty Acyl Chains Alter the Aggregation Behavior of an Amyloidogenic Peptide Derived from Human β(2)-Microglobulin. *J. Pept. Sci.* **2013**, *19*, 770–783.

(25) Macchi, F.; Hoffmann, S. V.; Carlsen, M.; Vad, B.; Imparato, A.; Rischel, C.; Otzen, D. E. Mechanical Stress Affects Glucagon Fibrillation Kinetics and Fibril Structure. *Langmuir* **2011**, *27*, 12539–12549.

(26) Sluzky, V.; Klibanov, A. M.; Langer, R. Mechanism of Insulin Aggregation and Stabilization in Agitated Aqueous Solutions. *Biotechnol. Bioeng.* **1992**, *40*, 895–903.

(27) Nielsen, L.; Khurana, R.; Coats, A.; Frokjaer, S.; Brange, J.; Vyas, S.; Uversky, V. N.; Fink, A. L. Effect of Environmental Factors on the Kinetics of Insulin Fibril Formation: Elucidation of the Molecular Mechanism. *Biochemistry* **2001**, *40*, 6036–6046.

(28) Foderà, V.; Librizzi, F.; Groenning, M.; van de Weert, M.; Leone, M. Secondary Nucleation and Accessible Surface in Insulin Amyloid Fibril Formation. *J. Phys. Chem. B* **2008**, *112*, 3853–3858.

(29) Mauri, S.; Volk, M.; Byard, S.; Berchtold, H.; Arnolds, H. Stabilization of Insulin by Adsorption on a Hydrophobic Silane Self-Assembled Monolayer. *Langmuir* **2015**, *31*, 8892–8900.

(30) Jorgensen, L.; Bennedsen, P.; Hoffmann, S. V.; Krogh, R. L.; Pinholt, C.; Groenning, M.; Hostrup, S.; Bukrinsky, J. T. Adsorption of Insulin with Varying Self-Association Profiles to a Solid Teflon Surface-Influence on Protein Structure, Fibrillation Tendency and Thermal Stability. *Eur. J. Pharm. Sci.* **2011**, *42*, 509–516.

(31) Brange, J.; Ribel, U.; Hansen, J. F.; Dodson, G.; Hansen, M. T.; Havelund, S.; Melberg, S. G.; Norris, F.; Norris, K.; Snel, L. Monomeric Insulins Obtained by Protein Engineering and Their Medical Implications. *Nature* **1988**, *333*, 679–682.

(32) Groenning, M. Binding Mode of Thioflavin T and Other Molecular Probes in the Context of Amyloid Fibrils-Current Status. *J. Chem. Biol.* **2010**, *3*, 1–18.

(33) Sethuraman, A.; Han, M.; Kane, R. S.; Belfort, G. Effect of Surface Wettability on the

Adhesion of Proteins. *Langmuir* **2004**, *20*, 7779–7788.

(34) Vörös, J. The Density and Refractive Index of Adsorbing Protein Layers. *Biophys. J.* **2004**, *87*, 553–561.

(35) Cubitt, R.; Fragnetto, G. D17: The New Reflectometer at the ILL. *Appl. Phys. A Mater. Sci. Process.* **2002**, *74*, 329–331.

(36) Campbell, R. A.; Wacklin, H. P.; Sutton, I.; Cubitt, R.; Fragneto, G. FIGARO: The New Horizontal Neutron Reflectometer at the ILL. *Eur. Phys. J. Plus* **2011**, *126*, 107.

(37) Nelson, A. Co-Refinement of Multiple-Contrast neutron/X-Ray Reflectivity Data Using MOTOFIT. *J. Appl. Crystallogr.* **2006**, *39*, 273–276.

(38) Nielsen, L.; Frokjaer, S.; Brange, J.; Uversky, V. N.; Fink, A. L. Probing the Mechanism of Insulin Fibril Formation with Insulin Mutants. *Biochemistry* **2001**, *40*, 8397–8409.

(39) Mauro, M.; Craparo, E. F.; Podestà, A.; Bulone, D.; Carrotta, R.; Martorana, V.; Tiana, G.; San Biagio, P. L. Kinetics of Different Processes in Human Insulin Amyloid Formation. *J. Mol. Biol.* **2007**, *366*, 258–274.

(40) Dong, M.; Hovgaard, M. B.; Xu, S.; Otzen, D. E.; Besenbacher, F. AFM Study of Glucagon Fibrillation via Oligomeric Structures Resulting in Interwoven Fibrils. *Nanotechnology* **2006**, *17*, 4003–4009.

(41) Sauerbrey, G. Verwendung von Schwingquarzen Zur Wägung Dünner Schichten Und Zur Mikrowägung. *Zeitschrift für Physik*, **1959**, *155*, 206–222.

(42) Hovgaard, M. B.; Dong, M.; Otzen, D. E.; Besenbacher, F. Quartz Crystal Microbalance Studies of Multilayer Glucagon Fibrillation at the Solid-Liquid Interface. *Biophys. J.* **2007**, *93*, 2162–2169.

(43) Olsson, A. L. J.; van der Mei, H. C.; Busscher, H. J.; Sharma, P. K. Acoustic Sensing of the Bacterium-Substratum Interface Using QCM-D and the Influence of Extracellular Polymeric Substances. *J. Colloid Interface Sci.* **2011**, *357*, 135–138.

(44) Morris, D. R. P.; Fatisson, J.; Olsson, A. L. J.; Tufenkji, N.; Ferro, A. R. Real-Time Monitoring of Airborne Cat Allergen Using a QCM-Based Immunosensor. *Sensors Actuators, B Chem.* **2014**, *190*, 851–857.

(45) Olsson, A. L. J.; van der Mei, H. C.; Johannsmann, D.; Busscher, H. J.; Sharma, P. K.

Probing Colloid-Substratum Contact Stiffness by Acoustic Sensing in a Liquid Phase. *Anal. Chem.* **2012**, *84*, 4504–4512.

(46) Dybwad, G. L. A Sensitive New Method for the Determination of Adhesive Bonding between a Particle and a Substrate. *J. Appl. Phys.* **1985**, *58*, 2789–2790.

(47) Pomorska, A.; Shchukin, D.; Hammond, R.; Cooper, M. A.; Grundmeier, G.; Johannsmann, D. Positive Frequency Shifts Observed upon Adsorbing Micron-Sized Solid Objects to a Quartz Crystal Microbalance from the Liquid Phase. *Anal. Chem.* **2010**, *82*, 2237–2242.

(48) Browning, K. L.; Griffin, L. R.; Gutfreund, P.; Barker, R. D.; Clifton, L. A.; Hughes, A.; Clarke, S. M. Specular Neutron Reflection at the Mica/water Interface – Irreversible Adsorption of a Cationic Dichain Surfactant. *J. Appl. Crystallogr.* **2014**, *47*, 1638–1646.

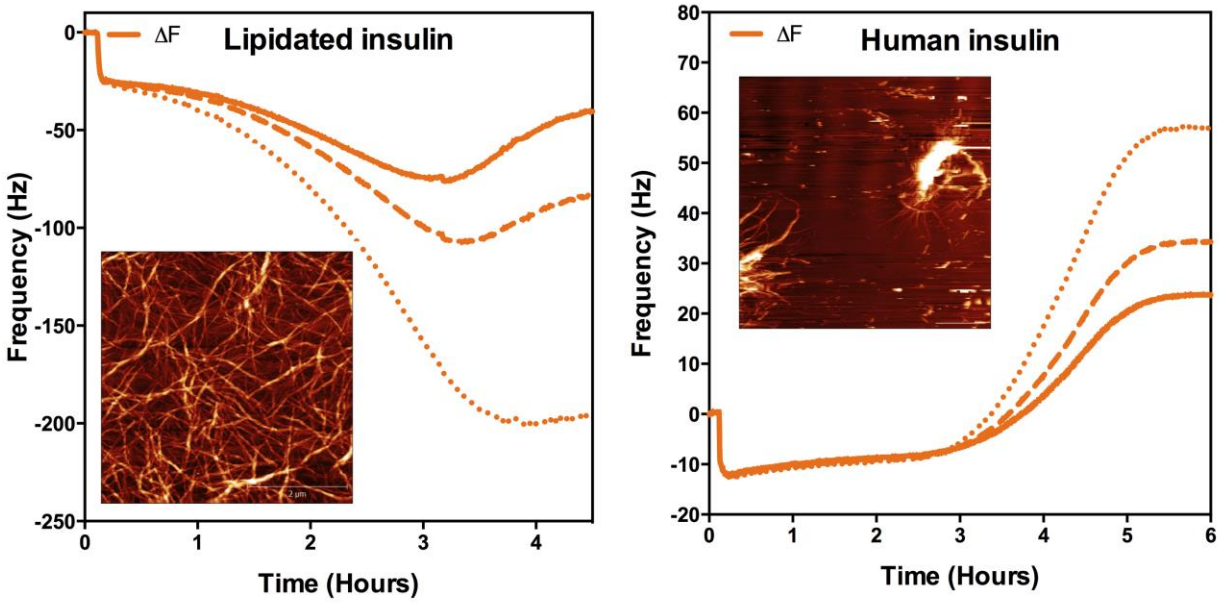


**Graphical abstract: For Table of Contents Only**